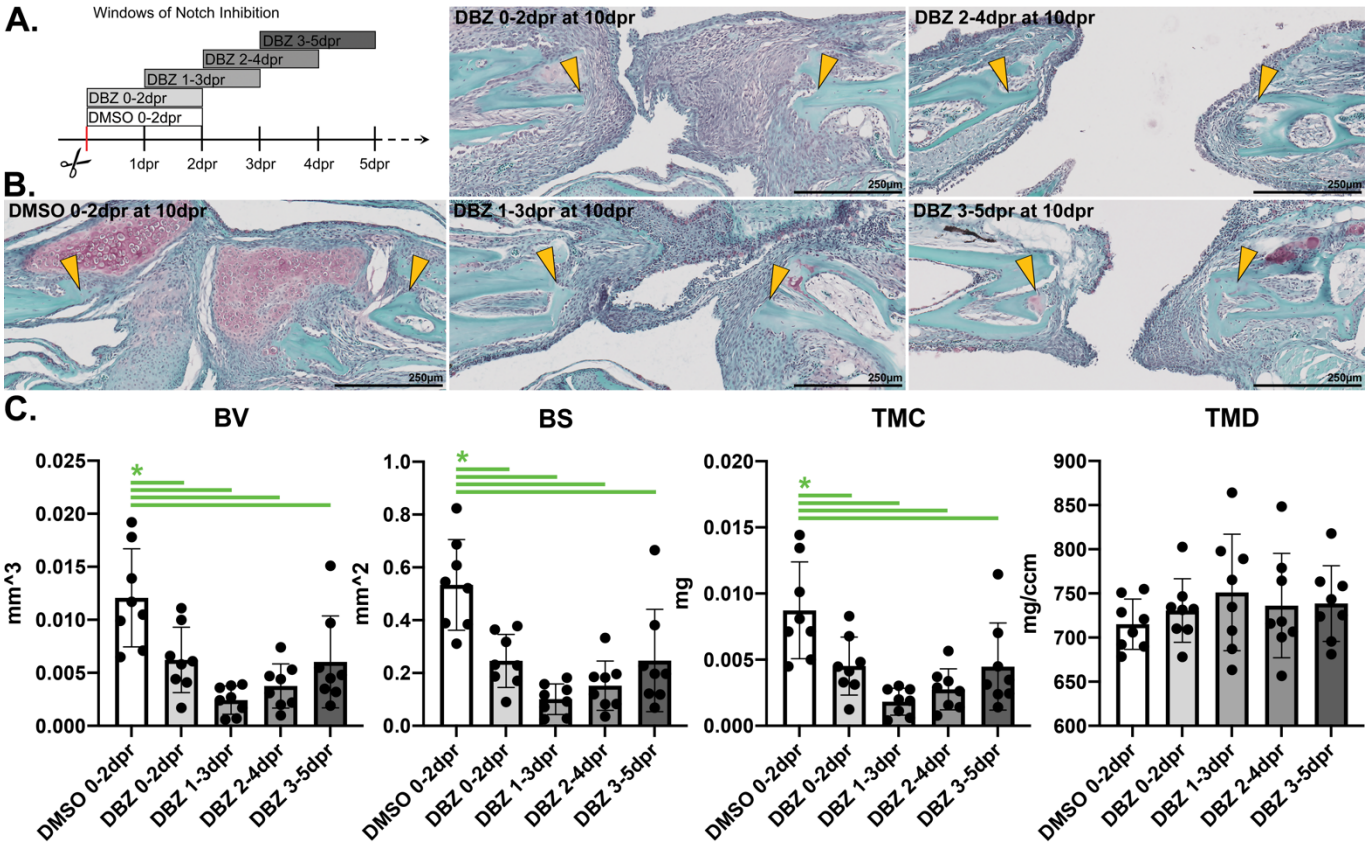

Fig. S1. Early Notch signaling is necessary for mandible regeneration. (A) A series of 48-hour DBZ treatments was used to identify the postoperative period most sensitive to Notch inhibition. (B) Stunted callus formation and an absence of cartilage was observed in all DBZ-treated groups by Safranin O histology, and 48-hour DBZ treatments conducted at 4 windows from 0-2 dpr to 3-5 dpr all result in soft tissue non-union. (C) Though DBZ windows were not sufficiently powered to reach statistical significance from each other via multiple comparisons, the 1-3 dpr period had the lowest mean regenerate bone at 32 dpr. Each graphed datapoint represents an individual fish (n=8 in each group), with bars depicting means and standard deviations. Green lines/asterisks represent statistical significance ($p<0.05$) using two-tailed t-tests with Welch's correction.

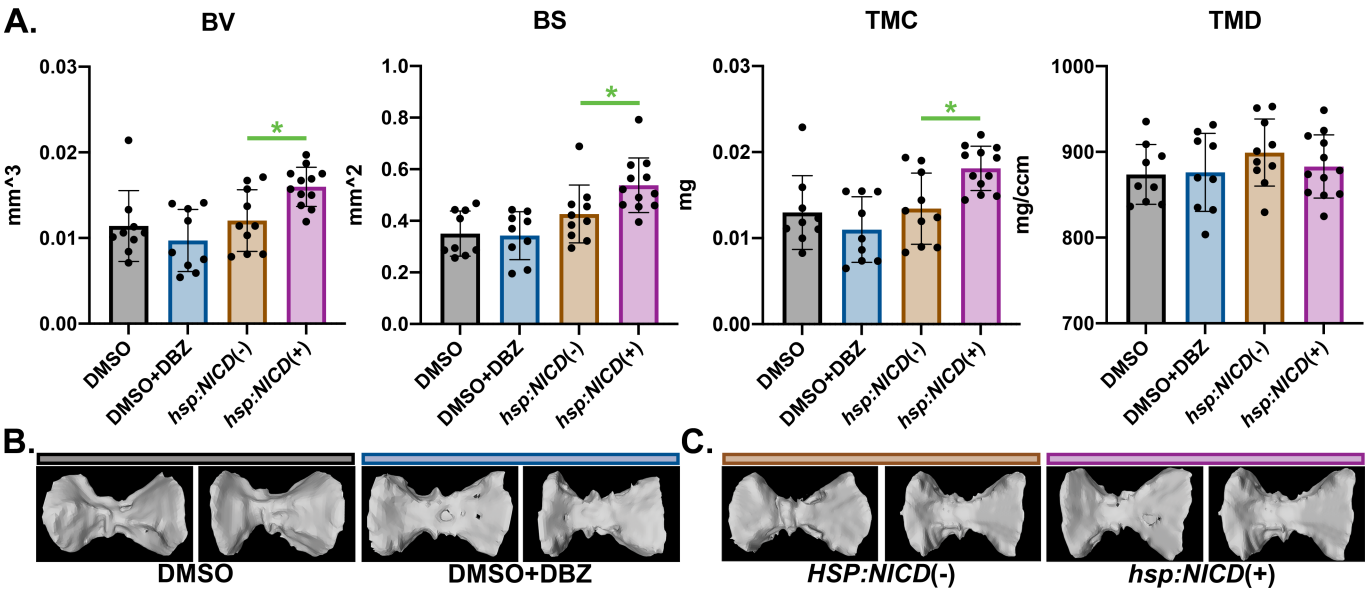

Fig. S2. Notch overactivation promotes vertebral bone accrual. µCT of the first precaudal/ thoracic (T1) vertebral body reveals off-target bone accrual following heat shock treatments in *hsp:NICD*+ animals relative to other groups. (A) As in the mandible, *hsp:NICD*+ animals acquire increased bone quantity but not density. BV was increased 32.8±19.0% (p=0.009), BS was increased 26.1±24.8% (p=0.028), and TMC was increased 34.9±19.2% (p=0.007) in the *hsp:NICD*+ group relative to the *hsp:NICD*(-) group. There was no vertebral phenotype in the DBZ group relative to the DMSO group. The 4 groups represent 9, 9, 10, and 12 animals, in order. (B-C) Two representative µCT surface renderings are shown for each group. Each graphed datapoint represents an individual fish, with bars depicting means and standard deviations. Green lines/asterisks represent statistical significance ($p<0.05$) using two-tailed t-tests with Welch's correction.

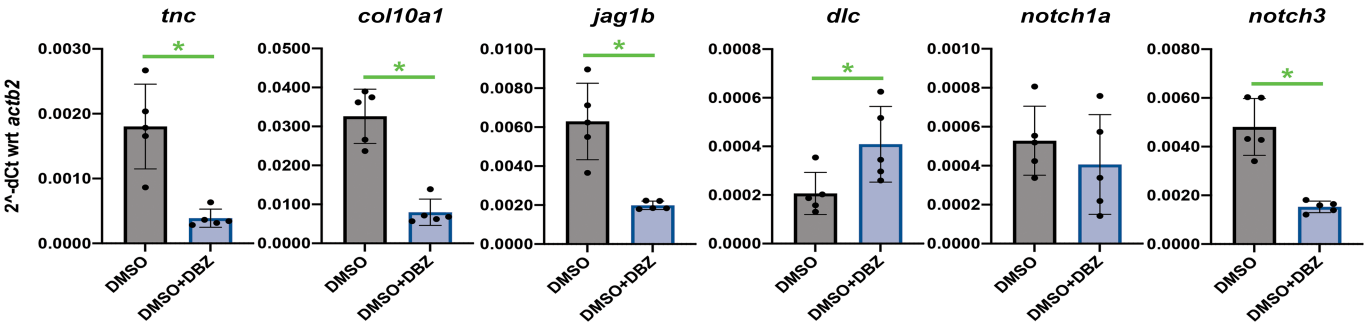

Fig. S3. Callus gene expression changes with DBZ treatment. (A) Whole-callus qPCR at 10 dpr in DMSO versus DMSO+DBZ treatment groups, continued from **Fig. 3D**. Each point represents a different pool of least 11 animals (n=5 pools in each group), with bars depicting means and standard deviations. Green lines/asterisks represent statistical significance ($p<0.05$) using two-tailed t-tests with Welch's correction.

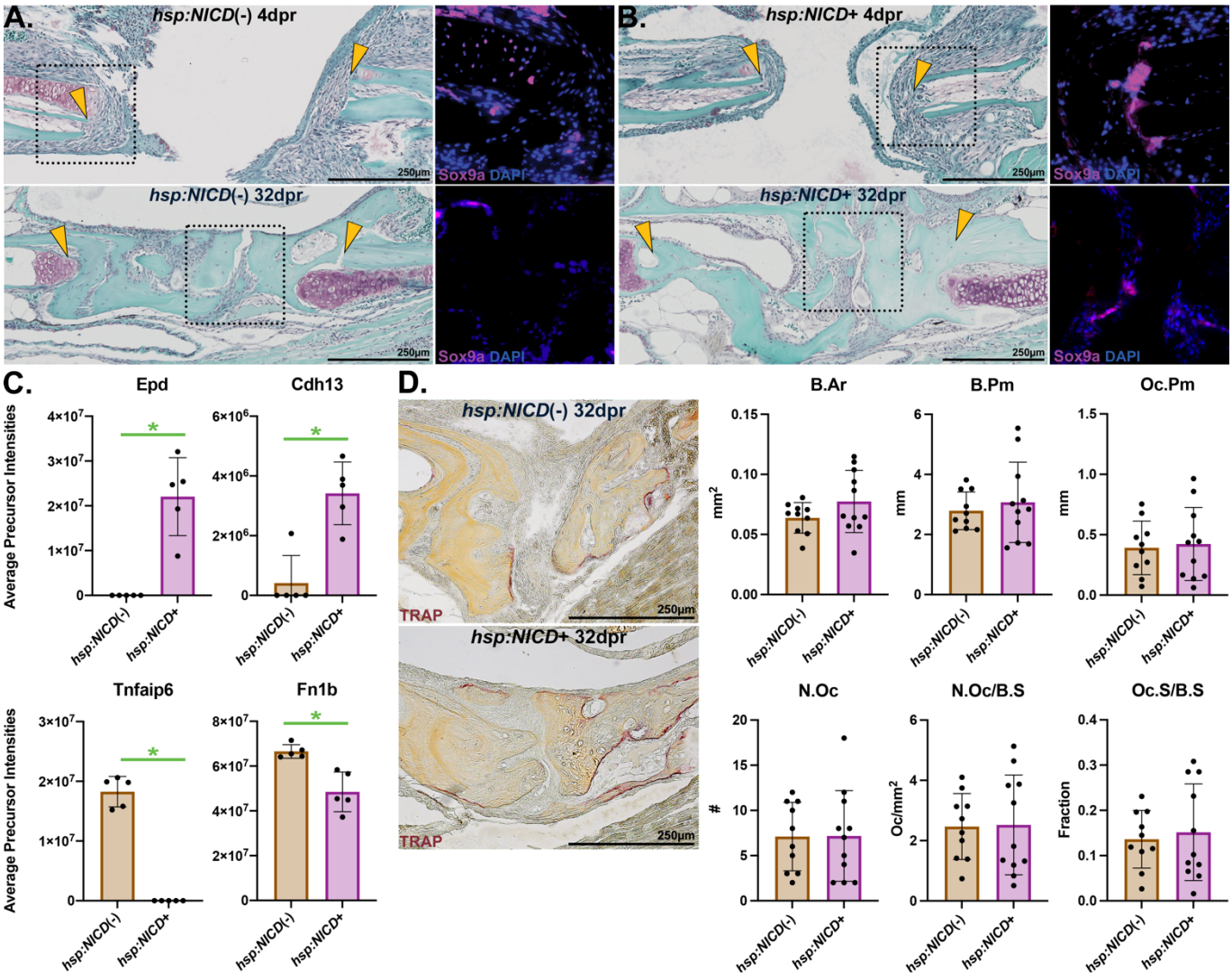

Fig. S4. Changes in mandible callus physiology by Notch overactivation. (A-B) Safranin O histology from *hsp:NICD*± animals show an absence of cartilage in both groups at 32 dpr, and more bone present in the *hsp:NICD*+ group (quantified by μCT in **Fig. 2**). The initial cellular response is positive for Sox9a. (C) Changes in the NICD+ callus proteome (continued from **Fig. 4**) include factors and extracellular matrix components associated with osteogenesis. Top hits include proteins with known functions in bone, such as the extracellular glycoprotein, ependymin (Epd; present only in all 5 *hsp:NICD*+ samples, $p<0.001$) (Pippin et al., 2021; Wagley et al., 2020), and the cell adhesion molecule, cadherin 13 (Cdh13; increased 8.3-fold, $p=0.001$) (Cheng et al., 1998; Yang et al., 2020). Tumor necrosis factor, alpha-

induced protein 6 (Tnfaip6; present only in all 5 *hsp:NICD*(-) samples, p<0.001), also known as Tsg6, an inflammation-induced secreted protein that sequesters BMP2 to inhibit osteoblast and odontoblast differentiation (Mahoney et al., 2008; Wang et al., 2020), was dramatically downregulated in the *hsp:NICD*+ calluses. Fibronectin (Fn1b; p=0.003) and numerous collagens were downregulated in the *hsp:NICD*+ group. (D) TRAP+ osteoclasts are present at 32 dpr in both groups, but histomorphometry was unremarkable for changes caused by NICD. Each graphed datapoint represents an individual fish, with bars depicting means and standard deviations (n=5 per group for proteomics, n=10 and 11 per group for TRAP). Green lines/asterisks represent statistical significance (p<0.05) using two-tailed t-tests with Welch's correction.

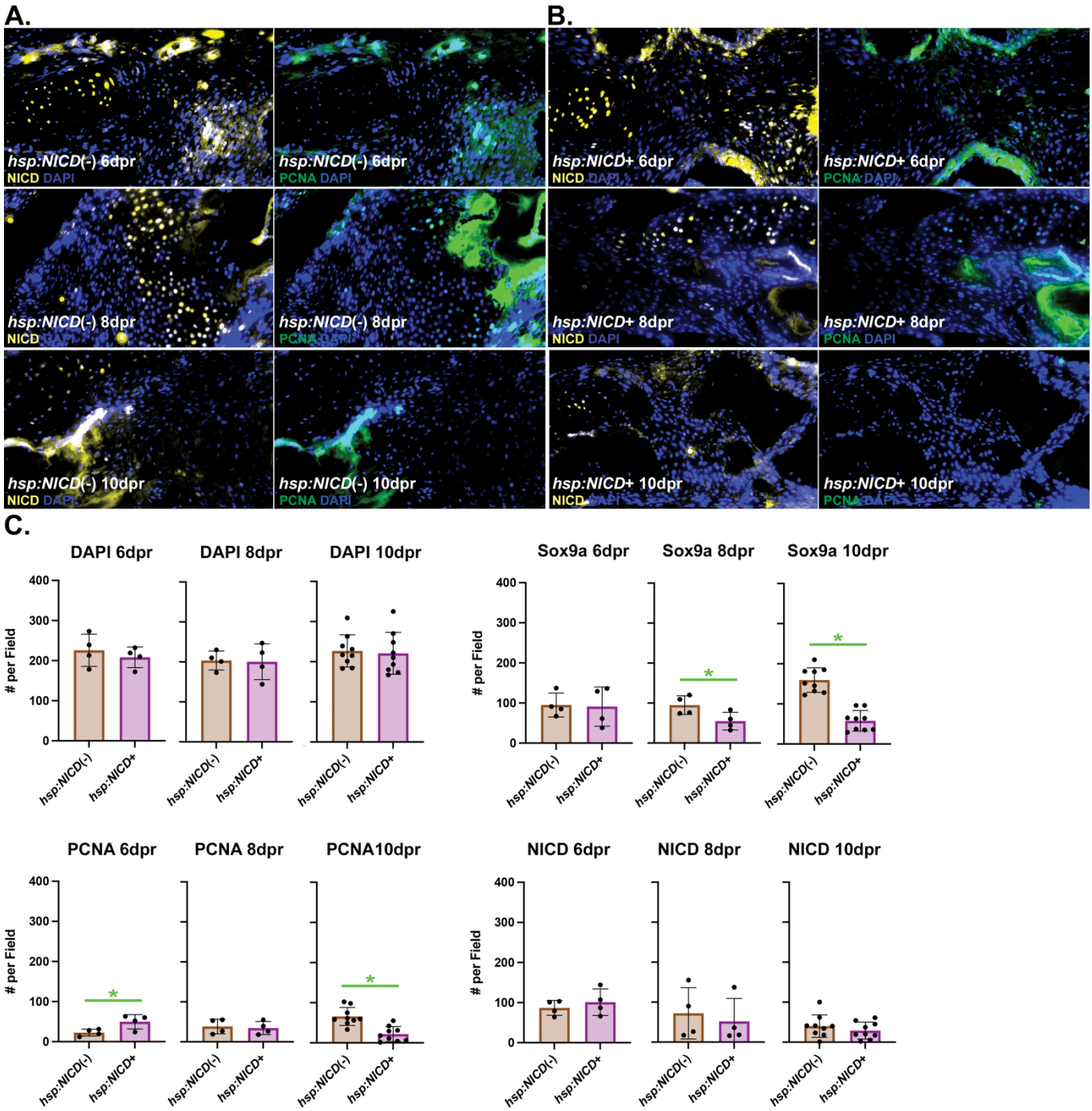

Fig. S5. A subpopulation of Sox9a+/NICD+ cells are proliferative. (A-B) α-NICD IHC (left column) and α-PCNA IHC (right column) from *hsp:NICD*± animals from the same sections and at the same magnification as α-Sox9a IHC in **Fig. 4**. All PCNA+ cells co-stain for NICD, but not all NICD+ cells co-stain for PCNA. (C) Quantitation of IHC shows decreased Sox9a positivity and altered PCNA

kinetics in the NICD+ group. The short half-life of NICD (Ilagan et al., 2011) resulted in a lack of detection of the ubiquitous transgene. Each graphed datapoint represents an individual fish, with bars depicting means and standard deviations (n=4 per group at 6 and 8 dpr, n=9 per group at 10 dpr). Green lines/asterisks represent statistical significance ($p<0.05$) using two-tailed t-tests with Welch's correction.

Table S1. qPCR primers. Forward and reverse primers for use with SYBR Green chemistry. The following abbreviations are used: *actb2* is β-actin 2, *bglap* is osteocalcin, *col10a1a* is collagen type X α1a, *col1a2* is collagen type II α2, *dla* is delta-like A, *dlb* is delta-like B, *dlc* is delta-like C, *dld* is delta-like D, *dll4* is delta-like 4, *her6* is hairy-related 6, *jag1a* is Jagged-1a, *jag1b* is Jagged-1b, *jag2a* is Jagged-2a, *jag2b* is Jagged-2b, *notch1a* is Notch receptor 1a, *notch1b* is Notch receptor 1b, *notch2* is Notch receptor 2, *notch3* is Notch receptor 3, *pcna* is proliferating cell nuclear antigen, *sox9a* is SRY-box transcription factor 9a, *sp7* is osterix, *spp1* is osteopontin, and *tnc* is tenascin C.

Gene	NCBI Accession	Forward Primer	Reverse Primer
actb2	NM_181601.5	GCAGAAGGAGATCACATCCCTGGC	CATTGCCGTCACCTTCACCGTTC
bglap	NM_001083857.3	TGAGTGCTGCAGAATCTCCTAA	GTCAGGTCTCCAGGTGCAGT
col10a1a	NM_001083827.1	CCTGTCTGGCTCATACCACA	AAGGCCACCAGGAGAAGAAG
col1a2	NM_182968.2	CTGGCATGAAGGGACACAG	GGGGTTCCATTTGATCCAG
dla	NM_130954.2	CTGTGAGAAACCTGGCGAGT	TCCATGTCAGTGCAGCTTCC
dlb	NM_130958.1	CTGTTGCAGTTGGTGGCTTC	CCAGACGACACTTGCACTCT
dlc	NM_130944.1	CATATTACCTGAGCCGCCGT	TCAAAGAGACGATTCCCGGC
dld	NM_130955.2	ACCCTTGCTCGAATGATGCT	CGCCGATCAGCACTAAAAGC
dll4			CTAAGCCAACGGCCAGAGAA
her6	NM_131079.2	GCTTGGGTCAGCTGAAAACG	GTGTTTAGGGCAGCGGTCAT
jag1a	NM_131861.1	GATGCGGGTATGTGAGGCTT	AGTGTGCCACAGGTGTTCAA
jag1b	NM_131863.2	AGAAAGCGTACCACTCTGGC	CCTTGTCTGCAGATCGCTGT
jag2a	XM_689725.8	GGCGGGACCGAACTGTAATA	GTTCATGGCTGTGTTGCAGG
jag2b	NM_131862.1	TCCCACTTGCGCTAAAGACAT	TTTACGCAAGGCTTCCCCAT
notch1a	NM_131441.1	GCCCGGATGGTCAGGTAAAA	CTCATTAATGCAGGTGCCGC
notch1b	NM_131302.2	ACACAAGGCCTGGAGTGTTC	CACAAATTCCTGCCGACCTG
notch2	NM_001115094.2	TCTAGACCAGGTCAGCCGAT	TTGAAACCTGCAAACCCACG
notch3	NM_131549.2	CCACGTTGCCAGTATCCAGT	TTTGCAGTAGTGCGTGTTGC
sox9a	NM_131643.1	GGAGCTCAGCAAAACTCTGG	AGTCGGGGTGATCTTTCTTG
sp7	NM_212863.2	GCGGCATCTATATTGGAGGA	AATCTCGGACTGGACTGGTG
spp1	NM_001002308.1	TGAAACAGATGAGAAGGAAGAGG	GGGTAGCCCAAACTGTCTCC
tnc	NM_130907.2	TTGGAGAAGGCCGGTTGCTAAAAT	CAGGGTTCAGGCCAGTCAGGATG

Table S2. Antibodies. Lot numbers for antibodies used, listed in order of first appearance in Histology Methods. All primaries used at 1:250 dilution, all secondaries used at 1:500 dilution.

Antibody	Lot
Novus NBP2-25158	7670-3
Abcam AB175477	GR3261221-8
GeneTex GTX48504	822101530
Sigma-Aldrich MoBU-1	3501021
BD Biosciences 559565	0349390
GeneTex GTX128370	41339
Invitrogen 13-3900	VS292226
Abcam A32849	WA307590
Abcam A11011	2277758
Abcam A11001	2284614
Abcam A11008	2284595
Abcam A32787TR	WI337286

Supplementary Methods

Proteomics

A 200 µg aliquot was removed from each total protein isolation and prepared for proteomics analysis via ultra-high performance liquid chromatography coupled to tandem mass spectrometry (UPLC-MS/MS) using a slightly modified Filter-Aided Sample Preparation protocol (Mara et al., 2020; Wisniewski et al., 2009). Briefly, proteins were diluted with UA buffer (8 M urea in 0.1 M Tris HCl, pH 8.5) and reduced with 25 mM dithiothreitol for 1.5 hr. The reduced protein aliquots were loaded onto Microcon YM-10 10 kD molecular weight cut-off filters pre-conditioned with bovine serum albumin (Sigma-Aldrich) and washed extensively. The filters were spun at 14,000 g for 40 min, the proteins were washed with a 200 µL aliquot of UA buffer, and then subject to another identical round of centrifugation. Proteins were then alkylated with 50 mM iodoacetamide in UA buffer for 15 min in the dark and centrifuged at 14,000 x g for 30 min. Proteins were equilibrated in UB buffer (8 M urea in 0.1 M Tris HCl, pH 8.0) via two consecutive wash and centrifugation steps at 14,000 x g for 30 min. Proteins were then resuspended in 40 µL UB buffer and placed into a new 1.5 mL Eppendorf Safe-Lock tube. The filters were washed twice with 40 µL aliquots of 0.1 M ammonium bicarbonate in water (Fisher Scientific) and washes were combined with the previously removed aliquot. All proteins were digested with endoproteinase LysC (Pierce) at a 1:50 (w/w) enzyme:protein ratio

for 16 hr at 37˚C. Samples were then diluted to yield urea concentrations <1 M using 0.1 M ammonium bicarbonate in water and further digested with trypsin (1:50 enzyme:protein, w/w) for 6 hr at 37˚C. Fully digested peptides were acidified using formic acid (Fisher Scientific) and subjected to desalting using Pierce C18 Peptide Desalting Spin Columns according to manufacturer's instructions. Dried peptides were resuspended in 0.1% formic acid in water and quantified using a NanoDrop One Spectrophotometer (Thermo Scientific, A280 reading, 1 Abs = 1.0 mg/mL).

Peptide samples were analyzed via UPLC-MS/MS using an UltiMate 3000 RSLCnano UPLC system coupled to a Q Exactive HF mass spectrometer (Thermo Scientific). A 180 min, 300 nL/min, linear reversed phase binary gradient (Solvent A: 0.1% formic acid in water, Solvent B: 0.1% formic acid in acetonitrile) was used to elute peptides directly into the Q Exactive HF instrument via positive mode electrospray ionization with +1.5 kV capillary voltage. The mass spectrometer was operated using the following parameters for precursor MS spectra: mass range 300 to 1800 m/z, 60,000 resolution, AGC target of 1e6, maximum ion time for 60 ms. A Top15 data-dependent mode for MS/MS acquisition used the following parameters: 15,000 resolution, AGC target of 1e5, isolation window of 2.0 m/z, normalized collision energy of 27, charge exclusion for unassigned, +1 and >+8 charge states, and a 30 s dynamic exclusion window.

All raw data were searched against the *Danio rerio* Uniprot reference proteome (UP000000437, accessed 05/17/2021, updated 01/29/2021) using MaxQuant (v1.6.10.43)(Cox and Mann, 2008). MaxQuant parameters included the following: trypsin enzyme specificity, minimum peptide length of 5 amino acids, maximum missed cleavage value of 2, PSM and Protein False Discovery Rate filters of 1%, variable modifications: oxidation of Met, acetylation of protein N-terminus, deamidation of Gln and Asn, and peptide N-terminal Gln to pyroGlu, plus a fixed modification of carbamidomethylation of Cys. All other parameters were left at default values. Label-free quantitation was achieved using the MaxLFQ algorithm. Maxquant output files were uploaded into Scaffold Q+S (v 5.0.0., Proteome Software Inc.) for visualization and further analysis.

In GOrilla, 69.7% of all input targets had a recognized GO term in the March 6, 2021 database. Enrichment score is equal to (b/n)/(B/N), where N is the total number of proteins, B is the total number of proteins associated with a specific GO term, n is the number of significantly dysregulated proteins, and b is the number of dysregulated proteins within a specific GO term.

Supplementary References

Cheng, S. L., Lecanda, F., Davidson, M. K., Warlow, P. M., Zhang, S. F., Zhang, L., Suzuki, S., St. John, T. and Civitelli, R. (1998). Human Osteoblasts Express a Repertoire of Cadherins, Which Are Critical for BMP‐2–Induced Osteogenic Differentiation. *J Bone Miner Res* 13, 633-644.

Cox, J. and Mann, M. (2008). MaxQuant enables high peptide identification rates, individualized ppb-range mass accuracies and proteome-wide protein quantification. *Nat Biotechnol.* 26, 1367-1372. doi:10.1038/nbt.151

Ilagan, M. X., Lim, S., Fulbright, M., Piwnica-Worms, D. and Kopan, R. (2011). Real-time imaging of notch activation with a luciferase complementation-based reporter. *Sci Signal* 4, rs7.

Mahoney, D. J., Mikecz, K., Ali, T., Mabilleau, G., Benayahu, D., Plaas, A., Milner, C. M., Day, A. J. and Sabokbar, A. (2008). TSG-6 regulates bone remodeling through inhibition of osteoblastogenesis and osteoclast activation. *J Biol Chem* 283, 25952-25962.

Mara, A. B., Gavitt, T. D., Tulman, E. R., Geary, S. J. and Szczepanek, S. M. (2020). Lipid moieties of Mycoplasma pneumoniae lipoproteins are the causative factor of vaccine-enhanced disease. *NPJ Vaccines* 5, 1-5.

Pippin, J A., Chesi, A., Wagley, Y., Su, C., Pahl, M. C., Hodge, K. M., Johnson, M. E., Wells, A. D., Hankenson, K. D. and Grant, S. F. (2021) CRISPR-Cas9-mediated genome editing confirms EPDR1as an effector gene at the BMD GWAS-implicated 'STARD3NL' locus. *JBMR Plus* 5:9.

Wagley, Y., Chesi, A., Acevedo, P. K., Lu, S., Wells, A. D., Johnson, M. E., Grant, S. F. and Hankenson, K. D. (2020). Canonical Notch signaling is required for bone morphogenetic protein-mediated human osteoblast differentiation. Stem Cells 38, 1332-1347.

Wang, Y., Yuan, S., Sun, J., Gong, Y., Liu, S., Guo, R., He, W., Kang, P. and Li, R. (2020). Inhibitory effect of the TSG-6 on the BMP-4/Smad signaling pathway and odonto/osteogenic differentiation of dental pulp stem cells. *Biomed Pharmacother* 128, 110266.

Wisniewski, J. R., Zougman, A., Nagaraj, N. and Mann, M. (2009). Universal sample preparation method

Yang, Y. R., Kabir, M. H., Park, J. H., Park, J.-I., Kang, J. S., Ju, S., Shin, Y. J., Lee, S. M., Lee, J. and Kim, S. (2020). Plasma proteomic profiling of young and old mice reveals cadherin-13 prevents age-related bone loss. *Aging* 12, 8652.